Computational Mechanics (2018) 62:1187–1198
https://doi.org/10.1007/s00466-018-1558-9

ORIGINAL PAPER

A 2D Daubechies finite wavelet domain method for transient wave response analysis in shear deformable laminated composite plates

C. V. Nastos[1] · T. C. Theodosiou[1] · C. S. Rekatsinas[1] · D. A. Saravanos[1]

Received: 12 July 2017 / Accepted: 12 February 2018 / Published online: 6 March 2018

Abstract
An efficient numerical method is developed for the simulation of dynamic response and the prediction of the wave propagation in composite plate structures. The method is termed finite wavelet domain method and takes advantage of the outstanding properties of compactly supported 2D Daubechies wavelet scaling functions for the spatial interpolation of displacements in a finite domain of a plate structure. The development of the 2D wavelet element, based on the first order shear deformation laminated plate theory is described and equivalent stiffness, mass matrices and force vectors are calculated and synthesized in the wavelet domain. The transient response is predicted using the explicit central difference time integration scheme. Numerical results for the simulation of wave propagation in isotropic, quasi-isotropic and cross-ply laminated plates are presented and demonstrate the high spatial convergence and problem size reduction obtained by the present method.

Keywords Daubechies wavelets · Wavelet-based elements · Composite plates · Wave propagation · Guided waves

1 Introduction

The development of fast and accurate numerical methods for analyzing the dynamic transient response and wave propagation in structural components has attracted substantial research interest. This is mainly driven by the design of non destructive evaluation (NDE) methods and passive and active structural health monitoring (SHM) systems based on linear and nonlinear ultrasonic waves, which require quick and robust simulations of wave propagation in pristine and damaged structures. Ultrasonic waves entail very high frequencies and wavenumbers, thus their numerical analysis based on traditional finite element methods (FEM) [1] and finite difference methods (FDM) [2] requires very fine spatial and temporal discretizations, which are usually computationally expensive and suffer from numerical shortcomings. Therefore, there is an emerging need for development of new modeling approaches and numerical tools which can provide solutions of improved accuracy with substantially reduced requirements for computer resources.

✉ D. A. Saravanos
saravanos@mech.upatras.gr

[1] Department of Mechanical Engineering and Aeronautics, University of Patras, 26500 Rion-Patras, Greece

Over the past decades, various numerical methods and techniques have been reported and extensively used for the simulation of transient dynamic phenomena in isotropic and composite structures. Fully analytical [3,4] and semi analytical finite element (SAFE) methods [5–7] result in accurate solutions, but they are applicable to limited types of structural configurations (e.g. semi infinite strips and plates) and boundary conditions. The time domain spectral element method (SEM) employs high order polynomial shape functions and Gauss–Lobatto–Legendre quadratures, which yield to fast and accurate solutions with consistent diagonal mass matrices [8,9]. However non uniform remeshing is required when increasing the order of polynomial shape functions, which is a time-consuming process.

The present paper presents a new numerical method, which implements Wavelet Scaling Functions (WSFs) for the spatial approximation of the displacement fields in 2D structures and explores its potential for the solution of wave propagation problems in isotropic and composite plates.

Numerous works have explored WSFs and wavelets as basis functions for the solution of differential equations and boundary value problems [10–12]. Patton and Marks have demonstrated the potential of wavelet-based FEA versus traditional approaches using a rod element in static and free vibration problems [13,14]. More recent works [15–17] employ Daubechies scaling functions as interpolating

functions to form stiffness matrices and load vectors for the static analyses of beams and thin plates. These works also suggest a way to transform generalized variables such as displacements and rotations from the wavelet to physical domain. The formulation of isotropic Eulerian beam and Mindlin–Reissner plate elements is described for static problems and the non shear locking behavior of the proposed method has been demonstrated [18]. In a different direction, wavelet spectral elements have been reported where Daubechies WSFs have been used to temporally approximate transient problems and reduce the PDEs to decoupled ODEs [19,20], which were solved with a spectral frequency domain element method. Apart from Daubechies wavelets, Deslauries-Dubuc interpolating wavelets, have been developed and used for the formulation of beam elements [21]. Although interpolets have higher vanishing moments than Daubechies WSFs, orthogonality is not satisfied, which is a crucial property for transient dynamic analysis as explained below. B-spline wavelets have been used to develop elements ranging from 1D first order shear (FOS) beam to higher order plate theories, for the investigation of static and free vibration problems [22–24]. Similarly to the interpolating wavelets, B-spline wavelet functions are non orthogonal as well. Recently, the authors introduced the Daubechies finite wavelet domain (FWD) method for the solution of transient dynamic problems in rods and strips [25,26]. The method incorporated first order shear and higher order beam theories for the rapid and efficient simulation of symmetric and anti-symmetric guided waves in composite strips. To our best knowledge no wavelet based methods have been reported for the analysis of wave propagation in isotropic and laminated composite plate structures.

The present paper, extends the FWD method to composite plates and expands the spatial approximation of the displacements in the wavelet domain in two dimensions. The first order shear deformation laminated plate theory (FSDT) [27] is adopted for the approximation of the local laminate response. Stiffness, consistent diagonal mass matrices and load vectors, are derived by integrating the equation of virtual displacements in the wavelet domain. The time response is predicted by using an explicit central difference time integration scheme. The performance of the developed Daubechies FWD method is assessed by predicting the propagation of the fundamental anti-symmetric wave (A_0) in aluminum, $[0/90/\pm 45]_s$ and cross-ply $[0_2/90_2]_s$ carbon/epoxy laminated plates. The high spatial convergence rate of various wavelet scaling functions is investigated and compared with 25-node and 9-node Lagrangian time domain spectral finite elements.

The present paper is organized as follows. Section 2 introduces the basic concepts of wavelet theory and properties of the Daubechies WSFs family. Section 3 describes the FWD method, its basic features and the formulation of a first order shear deformation laminated wavelet plate element. Section 4 presents numerical examples and convergence evaluations.

2 Daubechies wavelet: theoretical background

The selection of the most suitable WSF as interpolating function is an issue of much discussion [12]. Numerous wavelet families exist, each one with special characteristics. The Daubechies WSFs seems to be advantageous [28,29] for the approximation of state variables and the solution of variational forms of equations of motion, because they exhibit unique properties as functional bases, as summarized below. The Daubechies family of compactly supported orthonormal WSF $\phi(x)$, includes members of variable smoothness. As shown in Fig. 1, each WSF is nested at the point $x = 0$ and spans over a range of grid points, termed as the support domain. By definition, every WSF vanishes beyond its support domain. Several functional algorithms have been described for the construction procedure of Daubechies WSFs, wavelet functions and their respective derivatives [28,30], which are the initial step, in order to move on to wavelet analysis. After Daubechies WSFs were calculated by using recursive algorithms, much effort has been focused on the computation of wavelet integrals [31–33], which is a more challenging task because of the highly oscillatory nature especially of the higher order WSFs.

Scaling functions of the same order L can be defined either by translating the parent WSF at other integer points j, thus creating new WSFs of the type $\phi(x - j)$; or by shrinking/dilating the parent function to new WSFs $\phi(2^j x)$. WSFs

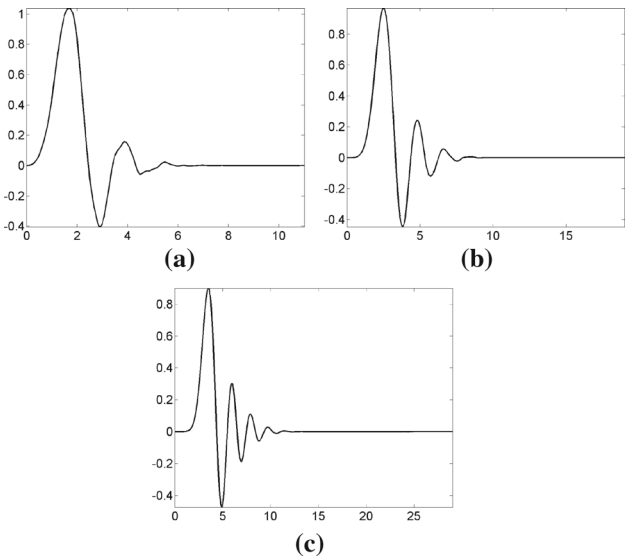

Fig. 1 Example of Daubechies Scaling functions $\phi(x)$. **a** DB6, **b** DB10, **c** DB15

possess additional properties which enhance their effectiveness as interpolation functions.

Compact Support Each WSF is confined within a bounded interval, which spans over a finite range of adjacent grid points, i.e $\phi(x)$ is defined $\forall\ x\ \in\ [0, 2L\ -\ 1]$. The value of the WSF beyond its compact support is zero by definition. Thus, the influence of a WSF as interpolation function is localized within the interval of compact support. The size of the interval of compact support depends on the order L of the parent WSF.

Orthonormality The integer translates of the WSF are orthonormal to each other, hence, the integer translates of WSFs form an orthonormal basis in the functional space.

$$\int_{-\infty}^{\infty} \phi(x-i)\cdot\phi(x-j)dx = \delta_{ij} \tag{1}$$

Vanishing Moments The number of vanishing moments defines the quality of the approximation and indicates the maximum degree of polynomial functions that can be exactly approximated by a specific WSF. A Daubechies WSF of order L has $L-1$ vanishing moments, which are the highest regarding 1^{st} generation wavelets.

Dilation Property Provided by the dilation equation,

$$\phi(x) = \sqrt{2}\cdot\sum_{k=0}^{2L-1} h_k\cdot\phi(2x-k) \tag{2}$$

where h_k is the set of $2L$ filter coefficients. The property is important, as it provides a relationship between the scaling function of a coarse approximation scale with the WSF of a finer approximation. The dilation property provides the basis for the calculation of WSF values at dyadic points and the WSF integrals.

3 The 2D finite wavelet domain method

In the present section the basic concepts of the FWD method are presented for the solution of transient dynamic wave problems in laminated composite plates. The approximation of displacements employing Daubechies WSFs as basis functions is described and its advantages are enumerated.

3.1 Approximation of field variables

The discretization of a rectangular plate of dimensions L_x, L_y is demonstrated in Fig. 2a. Additional nodes are introduced to the left and lower side of the physical domain, to account for the expansion of WSF over multiple grid points. The discretization shown corresponds to the case of a low order DB3 WSF, for demonstration purposes. To illustrate the approximation of displacement, we focus on an area between 4 consecutive nodes with coordinates $[x_i, y_i]$, $[x_{i+1}, y_i]$, $[x_{i+1}, y_{i+1}]$ and $[x_i, y_{i+1}]$. The mentioned area is catachrestically termed as element, because we use it to facilitate the approximation of field variables and the calculation of domain integrals. The relation between the global coordinate x and y to the local non-dimensional coordinate ξ and η is provided by

$$\xi = \frac{x-x_i}{l_x},\quad \xi\in[0,1] \tag{3}$$

$$\eta = \frac{y-y_i}{l_y},\quad \eta\in[0,1] \tag{4}$$

Because of the compact support mentioned previously, the displacement approximation in the physical domain $0\le x\le l_x, 0\le y\le l_y$ Fig. 2b, is calculated as

$$u(x,y,t) = \sum_{k,l=2-2L}^{0} \hat{u}_{kl}(t)\cdot\phi(\xi-k)\cdot\phi(\eta-l) \tag{5}$$

where l_x and l_y are the elemental lengths on the x and y axis respectively. $\phi(\xi-k)$, $\phi(\eta-l)$ are the integer translates of the WSF interpolation function; $\hat{u}_{kl}$ is a set of $(N+2L-1)^2$ unknown wavelet coefficients to be determined which corresponds to the nodes in the dash line area of Fig. 2b; k defines the column, l the row of the node and N the representative number of elements. These are the degrees of freedom (DOFs) in the wavelet space. Eq. (5) and Fig. 2b show that the approximation of field variables in the physical element requires a set of grid points in the corresponding support domain (Fig. 2b) where the wavelet coefficients are defined; this explains the selected terminology "finite wavelet domain method".

The introduced assembly reveals some advantages of FWD versus FEM. The FWD approximation of a field variable in an element requires DOFs from a range of nodes beyond the physical element, while in traditional FEA the approximation is local and strictly confined within each element. In fact, FWD method exploits the overlap of the influence domain for each element (Fig. 2a) and FWD elements use nodal DOFs involved in the field approximation of previous elements as well. Illustratively Fig. 2b shows the domain of influence for the shaded element. The amount of nodal information utilized for the approximation of a field variable within an element is larger than any traditional FE of the same approximation order. The amount of nodal information depends on the size of the influence domain, which in turn depends on the order of the selected WSF. Apparently, the obtained FWD approximation lies between a global Ritz type approximation and the local FEM approximation, hence, it is expected to blend advantages of both.

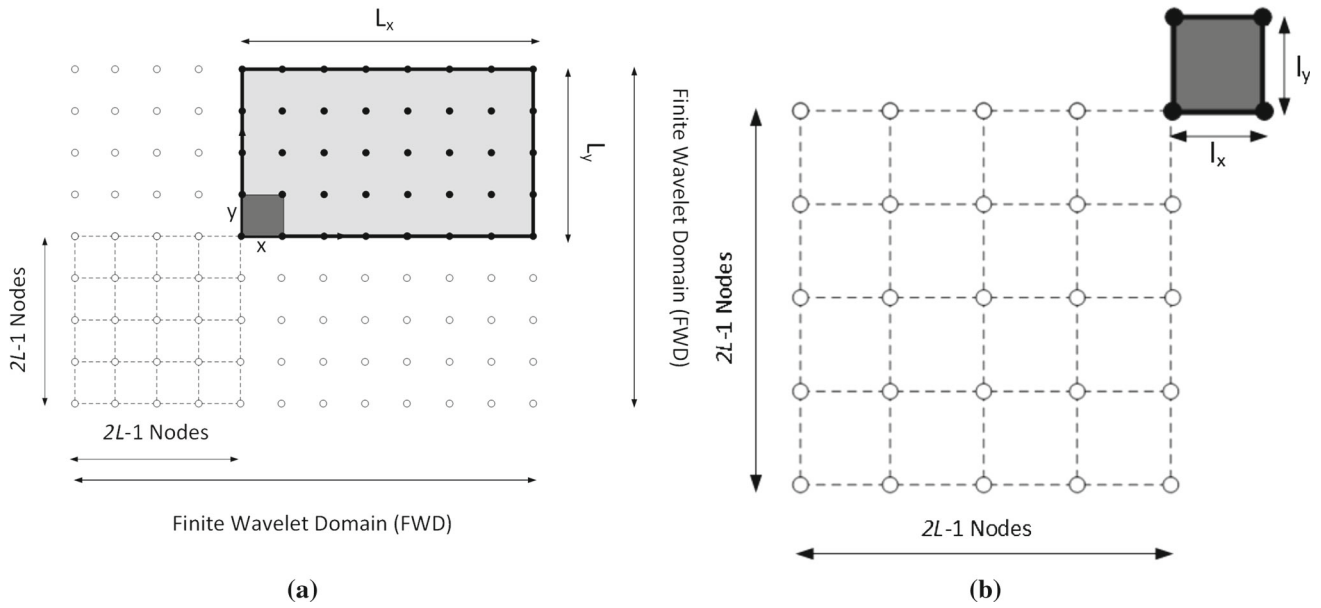

Fig. 2 Typical arrangement of grid points. **a** Grid points in the wavelet domain for the approximation of field variables in the physical plate area (light gray area). **b** Support nodes (dash line area) required for the approximation in the plate area confined by 4 consecutive nodes (dark gray area)

The FWD can improve the quality of approximation using either the h-method (keeping the order of WSF fixed and decreasing the nodal distance h) or the p-method (keeping the nodal distance fixed and increasing the order of the WSF). Due to the vanishing moment property of the WSF, an increase in the order of a DB WSF in Eq. (5), is related to a measurable improvement in the order of polynomial approximation. Specifically an increment in the order L of the WSF by 1, improves also the polynomial order of the approximation by 1. This increase in approximation order requires only the addition of totally two rows or columns of nodes per dimension in wavelet space (Fig. 2a) and no remeshing in the physical domain. On the contrary, an increment of the polynomial order of approximation in FEM requires the addition of one new node along each direction per element and full remeshing of the physical domain with new finite elements.

3.2 Wavelet-based element

The first order shear deformation laminated plate theory (FSDT) [27] outlined in the Appendix, provides the basis for the approximation of local laminate response. According to Eqs. (36–39), the principle of virtual displacements can be recast as

$$\int_{\Omega_0} \underset{\sim}{\delta\varepsilon}_L^T [\mathbf{K}_L] \underset{\sim}{\varepsilon}_L dxdy - \delta W + \int_{\Omega_0} \underset{\sim}{\delta u}_L^T [\boldsymbol{\rho}_L] \underset{\sim}{\ddot{u}}_L dxdy = 0 \tag{6}$$

where Ω_0 denotes the undeformed midplane, $\mathbf{K}_L$ is the material stiffness matrix, δW is the virtual work and is outlined in the Appendix (Eq. 38), $\boldsymbol{\rho}_L$ is the laminate density matrix, $\underset{\sim}{u}_L$ are the generalized displacements.

The approximation of the generalized strains in an element takes the form shown in Eq. (7),

$$\underset{\sim}{\varepsilon}_L = \begin{bmatrix} \varepsilon_x \\ \varepsilon_y \\ \varepsilon_{xy} \\ k_x \\ k_y \\ k_{xy} \\ \varepsilon_{yz} \\ \varepsilon_{xz} \end{bmatrix} = \sum_{k,l=2-2L}^{0} \begin{bmatrix} \boldsymbol{R}^{11} & \boldsymbol{R}^{12} & \boldsymbol{R}^{13} & \boldsymbol{R}^{14} & \boldsymbol{R}^{15} \\ \boldsymbol{R}^{21} & \boldsymbol{R}^{22} & \boldsymbol{R}^{23} & \boldsymbol{R}^{24} & \boldsymbol{R}^{25} \\ \boldsymbol{R}^{31} & \boldsymbol{R}^{32} & \boldsymbol{R}^{33} & \boldsymbol{R}^{34} & \boldsymbol{R}^{35} \\ \boldsymbol{R}^{41} & \boldsymbol{R}^{42} & \boldsymbol{R}^{43} & \boldsymbol{R}^{44} & \boldsymbol{R}^{45} \\ \boldsymbol{R}^{51} & \boldsymbol{R}^{52} & \boldsymbol{R}^{53} & \boldsymbol{R}^{54} & \boldsymbol{R}^{55} \\ \boldsymbol{R}^{61} & \boldsymbol{R}^{62} & \boldsymbol{R}^{63} & \boldsymbol{R}^{64} & \boldsymbol{R}^{65} \\ \boldsymbol{R}^{71} & \boldsymbol{R}^{72} & \boldsymbol{R}^{73} & \boldsymbol{R}^{74} & \boldsymbol{R}^{75} \\ \boldsymbol{R}^{81} & \boldsymbol{R}^{82} & \boldsymbol{R}^{83} & \boldsymbol{R}^{84} & \boldsymbol{R}^{85} \end{bmatrix} \cdot \begin{bmatrix} \hat{u}_{kl}^0 \\ \hat{\beta}_{x\,kl} \\ \hat{v}_{kl}^0 \\ \hat{\beta}_{y\,kl} \\ \hat{w}_{kl}^0 \end{bmatrix} \tag{7}$$

where

$$\mathbf{R}^{11} = \mathbf{R}^{33} = \mathbf{R}^{42} = \mathbf{R}^{64} = \mathbf{R}^{85} = \phi_{,x}(\xi - k) \cdot \phi(\eta - l) \tag{8}$$

$$\mathbf{R}^{23} = \mathbf{R}^{31} = \mathbf{R}^{54} = \mathbf{R}^{62} = \mathbf{R}^{75} = \phi(\xi - k) \cdot \phi_{,y}(\eta - l) \tag{9}$$

$$\mathbf{R}^{74} = \mathbf{R}^{82} = \phi(\xi - k) \cdot \phi(\eta - l) \tag{10}$$

and indices $k, l = 2 - 2L, ..., 0$ are symmetric. The remaining elements of matrix $[\mathbf{R}]$ are zero. Combining Eqs. (5, 6) equivalent expressions of virtual work and the corresponding stiffness $[\boldsymbol{K}_e]$ and mass $[\boldsymbol{M}_e]$ matrices, as well as surface traction vectors $[\boldsymbol{F}_{\tau e}]$ can be calculated for each FWD ele-

ment area as follows:

$$\delta\hat{\boldsymbol{U}}_e^T \cdot [\boldsymbol{K}_e] \cdot \hat{\boldsymbol{U}}_e = \int_0^{l_x}\int_0^{l_y}\left(\int_{-h/2}^{h/2} \delta\boldsymbol{\varepsilon}^T \cdot \boldsymbol{\sigma} dz\right) dxdy \quad (11)$$

$$\delta\hat{\boldsymbol{U}}_e^T \cdot [\boldsymbol{M}_e] \cdot \ddot{\hat{\boldsymbol{U}}}_e = \int_0^{l_x}\int_0^{l_y}\left(\int_{-h/2}^{h/2} \delta\boldsymbol{u}^T \cdot \rho \cdot \ddot{\boldsymbol{u}} dz\right) dxdy \quad (12)$$

$$\delta U_e^T \cdot [\boldsymbol{F}_{\tau e}] = \int_0^{l_x}\int_0^{l_y}\left[\delta\boldsymbol{u}^T \cdot \bar{\boldsymbol{\tau}}\right]_{-h/2}^{h/2} dxdy \quad (13)$$

where h denotes the thickness of the plate and $\hat{\boldsymbol{U}}_e$ is the generalized vector of wavelet coefficients involved in the elemental approximation of the displacements and rotations in Eq. (5)

3.2.1 Stiffness matrix

Incorporation of the approximated variables (Eqs. 37, 38, 39) into Eq. (36) yields the following symmetric elemental stiffness and mass matrices, Eqs. (14–21)

$$[\boldsymbol{K}_e^{klmn}] = \begin{bmatrix} \boldsymbol{K}_{e11}^{klmn} & \boldsymbol{K}_{e12}^{klmn} & \boldsymbol{K}_{e13}^{klmn} & \boldsymbol{K}_{e14}^{klmn} & \boldsymbol{K}_{e15}^{klmn} \\ \boldsymbol{K}_{e21}^{klmn} & \boldsymbol{K}_{e22}^{klmn} & \boldsymbol{K}_{e23}^{klmn} & \boldsymbol{K}_{e24}^{klmn} & \boldsymbol{K}_{e25}^{klmn} \\ \boldsymbol{K}_{e31}^{klmn} & \boldsymbol{K}_{e32}^{klmn} & \boldsymbol{K}_{e33}^{klmn} & \boldsymbol{K}_{e34}^{klmn} & \boldsymbol{K}_{e35}^{klmn} \\ \boldsymbol{K}_{e41}^{klmn} & \boldsymbol{K}_{e42}^{klmn} & \boldsymbol{K}_{e43}^{klmn} & \boldsymbol{K}_{e44}^{klmn} & \boldsymbol{K}_{e45}^{klmn} \\ \boldsymbol{K}_{e51}^{klmn} & \boldsymbol{K}_{e52}^{klmn} & \boldsymbol{K}_{e53}^{klmn} & \boldsymbol{K}_{e54}^{klmn} & \boldsymbol{K}_{e55}^{klmn} \end{bmatrix} \quad (14)$$

where

$$\begin{aligned}
\mathbf{K}_{e11}^{klmn} &= A_{11}\frac{l_y}{l_x}\mathbf{0}_{kl}^{11}\mathbf{\Gamma}_{mn}^{00} + A_{16}\mathbf{\Gamma}_{kl}^{10}\mathbf{\Gamma}_{mn}^{01} + A_{16}\mathbf{\Gamma}_{kl}^{01}\mathbf{\Gamma}_{mn}^{10} \\
&\quad + A_{66}\frac{l_x}{l_y}\mathbf{\Gamma}_{kl}^{00}\mathbf{\Gamma}_{mn}^{11} \\
\mathbf{K}_{e12}^{klmn} &= B_{11}\frac{l_y}{l_x}\mathbf{\Gamma}_{kl}^{11}\mathbf{\Gamma}_{mn}^{00} + B_{16}\mathbf{\Gamma}_{kl}^{10}\mathbf{\Gamma}_{mn}^{01} + B_{16}\mathbf{\Gamma}_{kl}^{01}\mathbf{\Gamma}_{mn}^{10} \\
&\quad + B_{66}\frac{l_x}{l_y}\mathbf{\Gamma}_{kl}^{00}\mathbf{\Gamma}_{mn}^{11} \\
\mathbf{K}_{e13}^{klmn} &= A_{16}\frac{l_y}{l_x}\mathbf{\Gamma}_{kl}^{11}\mathbf{\Gamma}_{mn}^{00} + A_{66}\mathbf{\Gamma}_{kl}^{10}\mathbf{\Gamma}_{mn}^{01} + A_{12}\mathbf{\Gamma}_{kl}^{01}\mathbf{\Gamma}_{mn}^{10} \\
&\quad + A_{26}\frac{l_x}{l_y}\mathbf{\Gamma}_{kl}^{00}\mathbf{\Gamma}_{mn}^{11} \\
\mathbf{K}_{e14}^{klmn} &= B_{16}\frac{l_y}{l_x}\mathbf{\Gamma}_{kl}^{11}\mathbf{\Gamma}_{mn}^{00} + B_{66}\mathbf{\Gamma}_{kl}^{10}\mathbf{\Gamma}_{mn}^{01} + B_{12}\mathbf{\Gamma}_{kl}^{01}\mathbf{\Gamma}_{mn}^{10} \\
&\quad + B_{26}\frac{l_x}{l_y}\mathbf{\Gamma}_{kl}^{00}\mathbf{\Gamma}_{mn}^{11} \\
\mathbf{K}_{e15}^{klmn} &= 0 \qquad (15) \\
\mathbf{K}_{e22}^{klmn} &= A_{55}\cdot l_x\, l_y \cdot \mathbf{\Gamma}_{kl}^{00}\mathbf{\Gamma}_{mn}^{00} + D_{11}\frac{l_y}{l_x}\mathbf{\Gamma}_{kl}^{11}\mathbf{\Gamma}_{mn}^{00} \\
&\quad + D_{16}\mathbf{\Gamma}_{kl}^{10}\mathbf{\Gamma}_{mn}^{01} + D_{16}\mathbf{\Gamma}_{kl}^{01}\mathbf{\Gamma}_{mn}^{10} + D_{66}\frac{l_x}{l_y}\mathbf{\Gamma}_{kl}^{00}\mathbf{\Gamma}_{mn}^{11} \\
\mathbf{K}_{e23}^{klmn} &= B_{16}\frac{l_y}{l_x}\mathbf{\Gamma}_{kl}^{11}\mathbf{\Gamma}_{mn}^{00} + B_{66}\mathbf{\Gamma}_{kl}^{10}\mathbf{\Gamma}_{mn}^{01} + A_{16}\mathbf{\Gamma}_{kl}^{01}\mathbf{\Gamma}_{mn}^{10} \\
&\quad + A_{66}\frac{l_x}{l_y}\mathbf{\Gamma}_{kl}^{00}\mathbf{\Gamma}_{mn}^{11} \\
\mathbf{K}_{e24}^{klmn} &= A_{45}\cdot l_x\, l_y \cdot \mathbf{\Gamma}_{kl}^{00}\mathbf{\Gamma}_{mn}^{00} + D_{16}\frac{l_y}{l_x}\mathbf{\Gamma}_{kl}^{11}\mathbf{\Gamma}_{mn}^{00} \\
&\quad + D_{12}\mathbf{\Gamma}_{kl}^{01}\mathbf{\Gamma}_{mn}^{10} + D_{66}\mathbf{\Gamma}_{kl}^{10}\mathbf{\Gamma}_{mn}^{01} + D_{26}\frac{l_x}{l_y}\mathbf{\Gamma}_{kl}^{00}\mathbf{\Gamma}_{mn}^{11} \\
\mathbf{K}_{e25}^{klmn} &= A_{45}\cdot l_x \cdot \mathbf{\Gamma}_{kl}^{00}\mathbf{\Gamma}_{mn}^{10} + A_{55}\cdot l_y \cdot \mathbf{\Gamma}_{kl}^{10}\mathbf{\Gamma}_{mn}^{00} \qquad (16) \\
\mathbf{K}_{e33}^{klmn} &= A_{66}\frac{l_y}{l_x}\mathbf{\Gamma}_{kl}^{11}\mathbf{\Gamma}_{mn}^{00} + A_{26}\mathbf{\Gamma}_{kl}^{10}\mathbf{\Gamma}_{mn}^{01} + A_{26}\mathbf{\Gamma}_{kl}^{01}\mathbf{\Gamma}_{mn}^{10} \\
&\quad + A_{22}\frac{l_x}{l_y}\mathbf{\Gamma}_{kl}^{00}\mathbf{\Gamma}_{mn}^{11} \\
\mathbf{K}_{e34}^{klmn} &= B_{66}\frac{l_y}{l_x}\mathbf{\Gamma}_{kl}^{11}\mathbf{\Gamma}_{mn}^{00} + B_{26}\mathbf{\Gamma}_{kl}^{10}\mathbf{\Gamma}_{mn}^{01} + B_{26}\mathbf{\Gamma}_{kl}^{01}\mathbf{\Gamma}_{mn}^{10} \\
&\quad + B_{22}\frac{l_x}{l_y}\mathbf{\Gamma}_{kl}^{00}\mathbf{\Gamma}_{mn}^{11} \\
\mathbf{K}_{e35}^{klmn} &= 0 \qquad (17) \\
\mathbf{K}_{e44}^{klmn} &= A_{44}\cdot l_x\, l_y \cdot \mathbf{\Gamma}_{kl}^{00}\mathbf{\Gamma}_{mn}^{00} + D_{66}\frac{l_y}{l_x}\mathbf{\Gamma}_{kl}^{11}\mathbf{\Gamma}_{mn}^{00} \\
&\quad + D_{26}\mathbf{\Gamma}_{kl}^{10}\mathbf{\Gamma}_{mn}^{01} + D_{26}\mathbf{\Gamma}_{kl}^{01}\mathbf{\Gamma}_{mn}^{10} + D_{22}\frac{l_x}{l_y}\mathbf{\Gamma}_{kl}^{00}\mathbf{\Gamma}_{mn}^{11} \\
\mathbf{K}_{e45}^{klmn} &= A_{44}\cdot l_x \cdot \mathbf{\Gamma}_{kl}^{00}\mathbf{\Gamma}_{mn}^{10} + A_{45}\cdot l_y \cdot \mathbf{\Gamma}_{kl}^{10}\mathbf{\Gamma}_{mn}^{00} \qquad (18) \\
\mathbf{K}_{e55}^{klmn} &= A_{55}\cdot \frac{l_y}{l_x} \cdot \mathbf{\Gamma}_{kl}^{00}\mathbf{\Gamma}_{mn}^{11} + A_{45} \cdot \mathbf{\Gamma}_{kl}^{01}\mathbf{\Gamma}_{mn}^{10} \\
&\quad + A_{45} \cdot \mathbf{\Gamma}_{kl}^{10}\mathbf{\Gamma}_{mn}^{01} + A_{44}\cdot\frac{l_x}{l_y}\cdot\mathbf{\Gamma}_{kl}^{11}\mathbf{\Gamma}_{mn}^{00} \qquad (19)
\end{aligned}$$

where $\mathbf{\Gamma}_{kl}^{ij}$, $0 \le i, j \le 1$ are the WSF quadratures in the element area, known as connection coefficients and represented as:

$$\mathbf{\Gamma}_{kl}^{ij} = \int_0^1 \phi^{(i)}(\xi - k)\cdot\phi^{(j)}(\xi - l)d\xi \quad (20)$$

The calculation of connection coefficients for Daubechies wavelets is thoroughly discussed on [26,30].

3.2.2 Mass matrix

The representative mass matrix is

$$[\mathbf{M}_e^{klmn}] = [\boldsymbol{\rho}_L]\cdot l_x l_y \cdot \mathbf{\Gamma}_{kl}^{00}\mathbf{\Gamma}_{mn}^{00} \quad (21)$$

The total matrices can be assembled from all elemental contributions in the context of Eqs. (11, 12, 13, 22) using typical procedures, which finally provide the discrete equation of motion expressed in the wavelet space.

$$[\boldsymbol{M}]\cdot\ddot{\hat{\boldsymbol{U}}}(t) + [\boldsymbol{K}]\cdot\hat{\boldsymbol{U}}(t) = \boldsymbol{F}(t) \quad (22)$$

In the above equation, $[\boldsymbol{M}]$, $[\boldsymbol{K}]$ are the total structural mass and stiffness matrices respectively, $\boldsymbol{F}$ is the external load

Table 1 Material properties and geometric parameters

	Symbol	Aluminum	Carbon/epoxy	Units
Material properties	E_{11}	70	121.469	GPa
	E_{22}/E_{33}	70	10.446	GPa
	G_{13}/G_{12}	26.923	5.109	GPa
	G_{23}	26.923	3.942	GPa
	$\nu_{13}/\nu_{12}/\nu_{23}$	0.3	0.32496	–
	ρ	2700	1578	kg/m^3
Plate Geometry	Length (x-axis)	0.6	0.5	m
	Width (y-axis)	0.6	0.5	m
	Thickness	2	2	mm

vector and $\hat{\boldsymbol{U}}(t)$ is the vector containing all unknown wavelet coefficients $\hat{u}_{nk}$ as referred in Eq. (5).

Additional advantages of the FWD method are realized in the synthesis of the mass matrix $\left[\mathbf{M}_e^{klmn}\right]$. The orthogonality of WSFs combined with their compact support yield diagonal connection coefficients ($\mathbf{\Gamma}_{kl}^{00} = \delta_{kl}$) and consequently diagonal consistent mass matrix [**M**] in Eq. (21) for symmetric laminates. Due to the compact support of the WSFs, the stiffness matrices are symmetric, sparse and narrow-banded, which enables fast and accurate solution of large-size static and dynamic problems. On the other hand, on static problems, or in dynamic problems involving implicit time integration, the efficiency of local FEM regarding stiffness matrix inversion may be better. However, the consideration of the present FWD approach may present other benefits versus local FEM, e.g. C1 approximation of displacement, improved calculation of strains, free shear locking behavior which are beyond the motivation and scope of the present paper and should be addressed in future works.

3.3 Explicit time integration

One of the main advantages of the FWD method is its capability to provide diagonal consistent mass matrices, due to the orthogonality of Daubechies WSFs. This feature yields a clear advantage in the implementation of central difference explicit time integration scheme.

$$\frac{1}{\Delta t^2}\left[\mathbf{M}\right]\cdot\mathbf{U}\left(t+\Delta t\right) = \mathbf{R} \tag{23}$$

$$\mathbf{R} = \mathbf{F}\left(t\right) - \left(\left[\mathbf{K}\right] - \frac{2}{\Delta t^2}\left[\mathbf{M}\right]\right)\cdot\mathbf{U}(t) - \frac{1}{\Delta t^2}\left[\mathbf{M}\right]\cdot\mathbf{U}\left(t-\Delta t\right) \tag{24}$$

The solution of Eq. (23) requires inversion of the mass matrix at every time step for the calculation of the generalized displacement vector at the next time step $\mathbf{U}(t+\Delta t)$. The availability of a diagonal consistent mass matrix eliminates the need to employ lump-mass matrices or other numerical techniques to achieve approximate mass matrix diagonalization. Hence, the solution of Eqs. (23–24) is expected to be much faster and accurate compared to traditional explicit FEA.

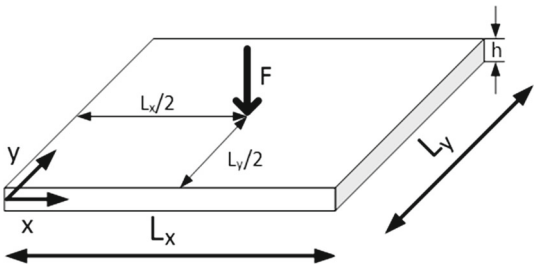

Fig. 3 Applied excitation of transverse point load on the center of the plates

4 Numerical results

The simulation of the fundamental anti-symmetric A_0 wave generation and propagation, which is crucial in many applications including the design of NDE and SHM methods and impact loading response, is a very challenging task, since it typically requires fine spatial discretization to capture the high wavenumbers, the dispersive characteristics, the amplitude and the group velocity of the propagating wave. Therefore the performance of the introduced FWD method is assessed on the prediction of ultrasonic A_0 wave propagation. Three cases of plates are examined: (1) aluminum isotropic plates, (2) $[0/90/\pm 45]_s$ and (3) cross-ply $[0_2/90_2]_s$ laminated carbon/epoxy plates. The properties and the geometry of the investigated plates are shown on Table 1. The results of the FWD method are compared with 25-node and 9-node Lagrangian Time Domain Spectral Finite Elements (TDSFE) [34].

The three plate cases are considered to be fully clamped at all four free edges (CCCC). Waves are excited by a concentrated transverse force, acting at the center ($x = \frac{L_x}{2}$, $y = \frac{L_y}{2}$) of each plate (Fig. 3), in the form of a 5 cycle Hanning win-

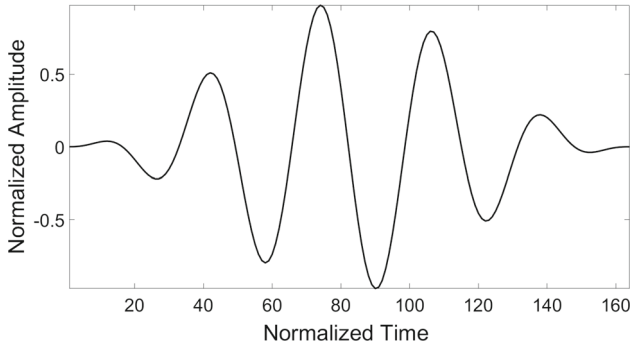

Fig. 4 Applied excitation using normalized amplitude

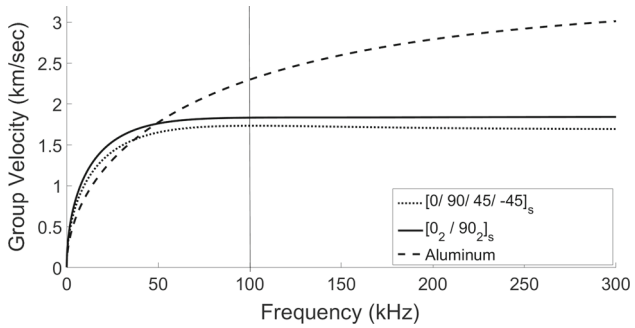

Fig. 5 Dispersion curves of the A_0 wave mode along the x-axis for the three plates

dowed narrowband pulse with central frequency of 100 kHz, as shown in Fig. 4. FWD models with DB6, DB10 and DB15 WSFs are used to predict the wave propagation. Figure 5 shows the dispersion curves of the first anti-symmetric mode for each laminate along the x-axis of a semi-infinite plate, predicted by a semi-analytical method [35]. At the detected central frequency of 100 kHz, the wave propagation in the aluminum plate is more dispersive compared to the composite plates.

The convergence rate and accuracy are determined by comparing the obtained solutions to a reference response, predicted by a converged model of the 9 node TDSFE corresponding to meshes of 1965604 for isotropic and 850084 nodes for laminated plates. Each investigated model is considered to have converged, when the root mean square (RMS) error of a snapshot along the x-axis for the aluminum and the $[0/90/\pm 45]_s$ case and along the y-axis for the cross-ply case at $t = 0.08$ ms and $t = 0.1$ ms respectively, with respect to the previous discretization was lower than 5%. The RMS calculation is indicated in Eq. (25), where n is the number of the compared interpolated points, u_{ref} is the reference solution and u_p is the predicted solution from the FWD and TDSFE models. As for the temporal discretization, the stable time step Δt (Eq. 26) applied in each analysis, is calculated by the respective maximum eigen-frequency f_{max} of each

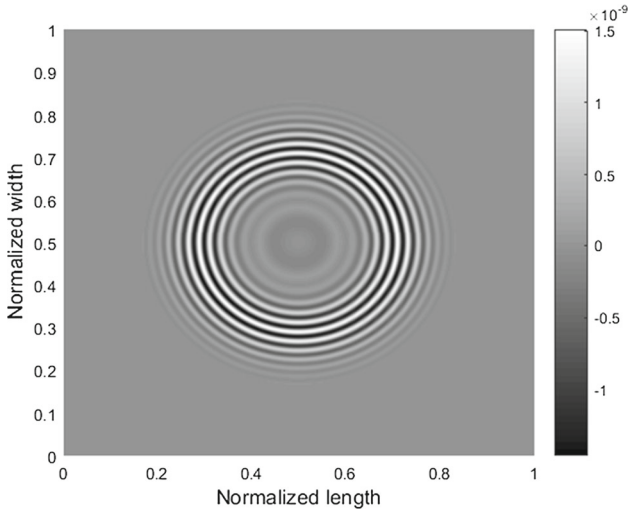

Fig. 6 Transverse displacement snapshot of A_0 wave mode propagation on the aluminum square plate at $t = 0.08$ ms

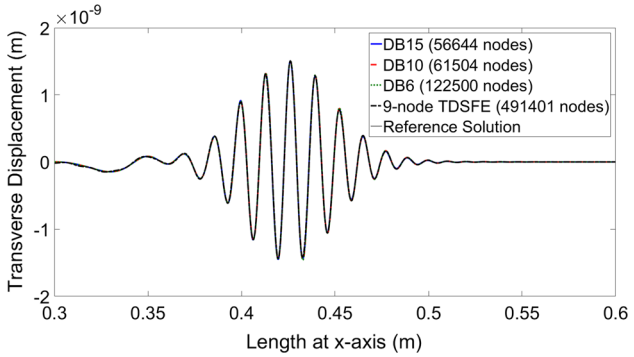

Fig. 7 Predicted A_0 mode for the aluminum plate at $t = 0.08$ ms and at $(x, \frac{L_y}{2})$ with $x \in [\frac{L_x}{2}, L_x]$ upon convergence of all FWD models and TDSFEs

structure.

$$RMS = \sqrt{\frac{\sum_{i=1}^{n}(u_{ref}^i - u_p^i)^2}{\sum_{i=1}^{n}(u_{ref}^i)^2}} \tag{25}$$

$$\Delta t = \frac{1}{4 \cdot f_{max}} \tag{26}$$

This criterion ensures the wave propagation characteristics, such as time of flight (ToF), frequency, amplitude and group/phase velocity are correctly depicted.

4.1 Case 1: aluminum plate

The predicted response of the aluminum square plate by a converged mesh of DB6 WSFs, is shown in Fig. 6 and illustrates a snapshot of the first anti-symmetric mode propagation at $t = 0.08$ ms.

Table 2 The required number of nodes using different Daubechies WSFs and the resultant relative gains (in parenthesis) versus TDSFE elements for a converged A_0 mode prediction

Element type	Required number of nodes Aluminum	$[0/90/\pm 45]_s$	Cross ply
DB15	56,644 (11.5%)	43,264 (20.4%)	43,264 (12.0%)
DB10	61,504 (12.5%)	56,644 (26.7%)	56,644 (15.7%)
DB6	122,500 (24.9%)	84,100 (39.6%)	108,900 (30.1%)
25-node TDSFE	148,225 (30.2%)	72,361 (34%)	108,241 (30%)
9-node TDSFE	491,401 (100%)	212,521 (100%)	361,201 (100%)

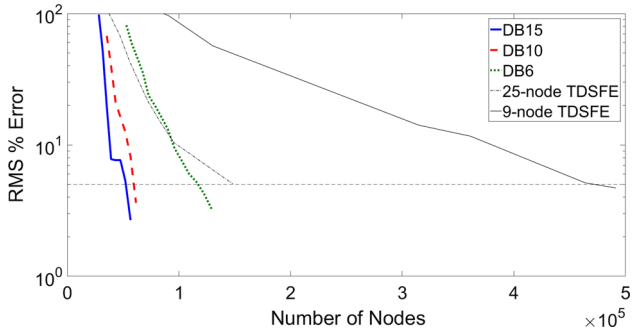

Fig. 8 Convergence rate (RMS % error versus number of nodes) for the prediction of A_0 wave propagation on the aluminum plate using the FWD method with various DB scaling functions

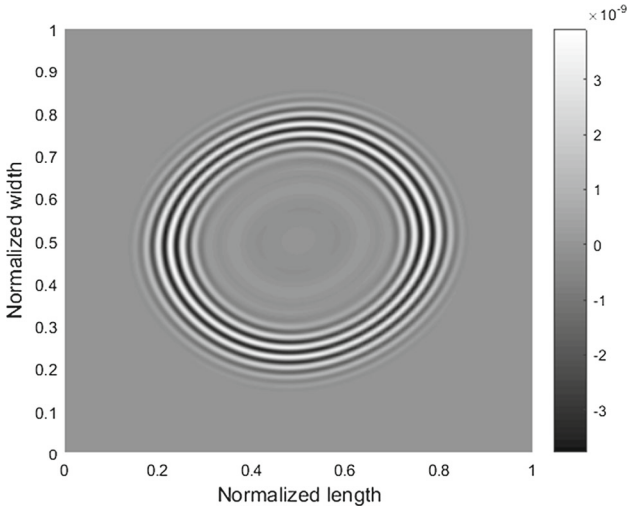

Fig. 9 Transverse displacement snapshot of A_0 wave mode propagation on $[0/90/\pm 45]_s$ square plate at $t = 0.1$ ms

Figure 7 shows the converged transverse displacement solutions along the x-axis at $t = 0.08$ ms predicted by the implementation of various WSFs and the TDSFE model. Apart from illustrating the accuracy of the 2D Daubechies FWD method, Fig. 7 also shows the high convergence rate of the FWD method in comparison with the reference TDSFE. Table 2 shows the number of nodes that each WSF requires to converge to the reference solution and the respective relative gains, versus the number of the required nodes by the TDSFEs. For the FWD models, the presented number of nodes concern both the physical domain nodes plus the extra wavelet domain nodes to have a fairer comparison with the TDSFEs. Clearly, as the wavelet order increases, less nodes are required to obtain a converged solution. In order to further support the fast convergence rate and the very small number of nodes that 2D Daubechies FWD elements require, a convergence study is presented on Fig. 8. The study is conducted until all four models have been converged with the criterion of RMS$\leq$ 5%. The RMS study (Fig. 8) clearly shows the superiority of FWD elements against TDSFEs on the convergence rate and thus on the matrix system minimization. The curve of RMS % Error versus nodes for the 25-node TDSFE seems to be bilinear and as the solution leads to convergence the slope decreases. This fact also supports the high convergence of the FWD models in more demanding dispersive cases.

Table 2, Figs. 7 and 8 clearly show that the usage of 2D Daubechies elements offers a much smaller size of system equations (Eq. 24) with diagonal mass matrix. About a quarter of nodes are required for similar convergence of a low order DB6 FWD element compared to a 9-node TDSFE. As the order of Daubechies WSF increases, substantially less nodes are needed to predict a converged solution, which illustrates the highly improved numerical performance of the FWD method in comparison with the TDSFEs or FEA and supports that the FWD method is a beneficial numerical tool for rapid and accurate numerical modeling of transient structural response.

4.2 Case 2: $[0/90/\pm 45]_s$ plate

The proposed FWD method is used to predict the first anti-symmetric A_0 mode in a $[0/90/45/-45]_s$ carbon/epoxy laminated plate. Figure 9 depicts the converged prediction of the first anti-symmetric mode A_0 contour plot at $t = 0.1$ ms, calculated by DB6 WSFs and excited at 100kHz.

The convergence of Daubechies FWD method, as the order of WSF increases, is shown in Figs. 10a, b and 11. Figure 10a shows a cross-section from the contour plot in (Fig.9) along the x-axis, i.e at $(x, \frac{L_y}{2})$ with $x \in [\frac{L_x}{2}, L_x]$. Apart from the converged predictions of all cases, which prove the cor-

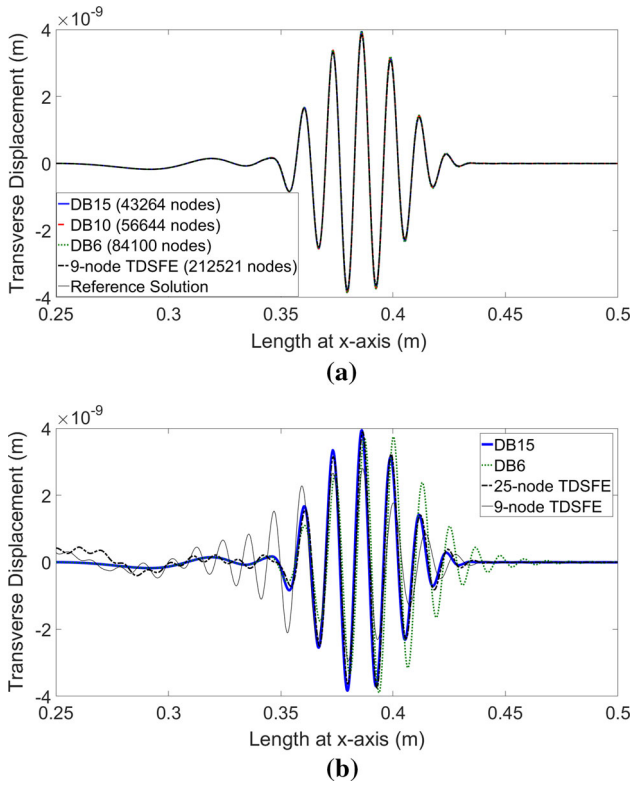

Fig. 10 A_0 wave mode predictions for the $[0/90/\pm 45]_s$ carbon/epoxy plate at $t = 0.1$ ms and at $(x, \frac{L_y}{2})$ with $x \in [\frac{L_x}{2}, L_x]$. **a** Upon convergence of all FWD models and TDSFEs; **b** using a grid of 43,264 nodes

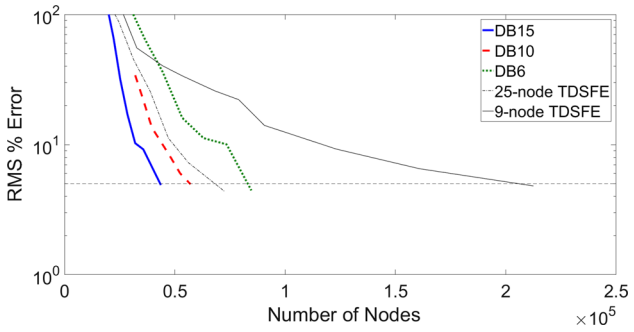

Fig. 11 Resultant RMS % error versus number of nodes for the FWD method using various DB scaling functions for the prediction of wave propagation in $[0/90/\pm 45]_s$ plate

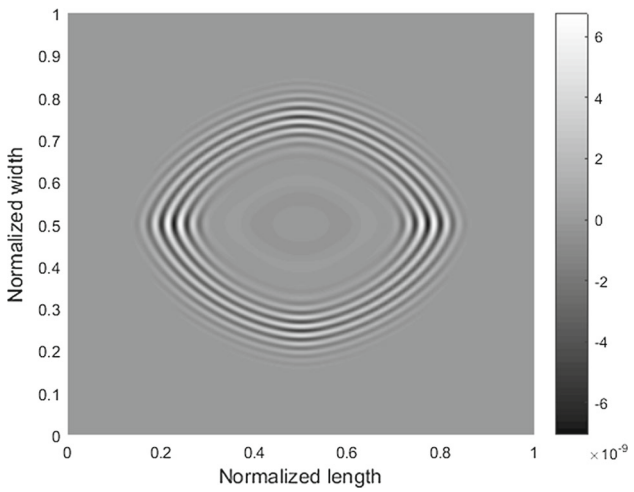

Fig. 12 Transverse displacement snapshot of A_0 wave mode propagation on a cross-ply square plate at $t = 0.1$ ms

rectness of the 2D FWD, Figs.10a, 11 and Table 2 also show the high convergence rate of the FWD method versus the TDSFE. The low order DB6 FWD element requires approximately one half of the nodes required by the 9-node TDSFE to converge at same solution. Additionally, it is clearly depicted that as the wavelet order increases, a smaller discretization is required to obtain a converged solution, yielding smaller size of system equations (Eq. 23). Figure 10b illustrates the obtained results by the DB6, DB15 and TDSFE models when they use the discretization (43,264 nodes) of the converged DB15 FWD model indicating substantial errors in the prediction of time of flight (ToF), amplitude and spurious dissipation of the investigated wave packet.

4.3 Case 3: cross-ply plate

The convergence rate and accuracy of the present FWD method is finally evaluated on a cross-ply $[0_2/90_2]_s$ carbon/epoxy laminated plate. Figure 12 shows the prediction of the propagating A_0 waves on the cross-ply plate, calculated by a converged mesh of DB6 WSFs. The FWD captures the strong directionality in group velocity, wavelength and dispersive characteristics of the A_0 wave packet.

Figure 13a, b shows the predicted propagation of the wave from the middle of the plate along the y-axis and x-axis respectively. As shown in Figs. 12 and 13 the wave characteristics of the A_0 wave depend on the propagating direction. The wave propagation along 90^0 seems to be more dispersive than the propagation along 0^0, hence the former requires higher number of nodes to obtain a converged solution. The fast convergence of the 2D Daubechies FWD model, is further quantified in the RMS study presented in Fig. 14 and in Table 2. The FWD models provide substantial reductions in the required number of nodes, thus lead to substantially reduced model sizes for the simulation of structural transient response.

In summary, the FWD method seems to perform almost two times better in more demanding cases involving dispersive guided wave propagation, as presented in Sect. 4.1. In all cases, a drastic reduction of nodes and as a result a reduction of the discrete system size is observed by the proposed FWD models. DB6 is comparable on the more demanding cases and inferior on simple cases such as the $[0/90/\pm 45]_s$

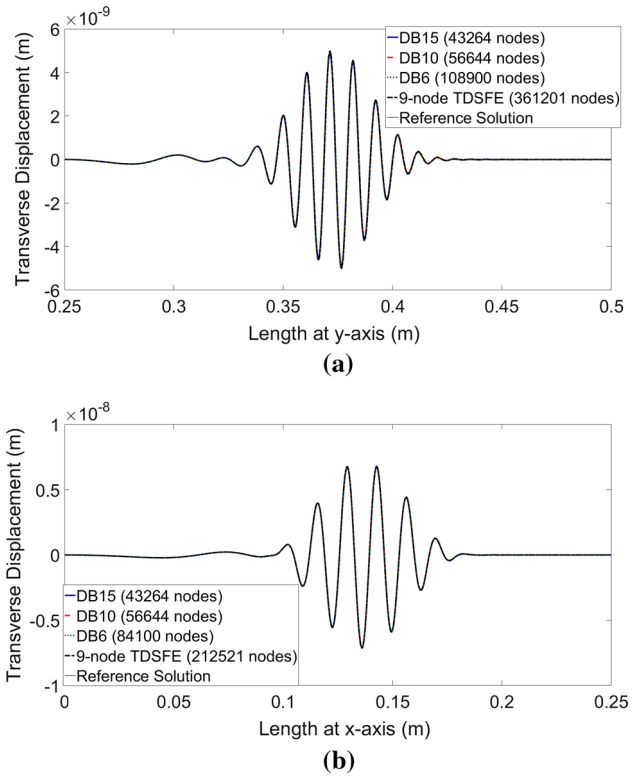

Fig. 13 Predicted A_0 wave mode for the cross ply carbon/epoxy plate at $t = 0.1$ ms upon convergence of all FWD models and TDSFEs. **a** Along y axis (width axis) $(\frac{L_x}{2}, y)$ with $y \in [\frac{L_y}{2}, L_y]$ **b** along x axis (length axis) $(x, \frac{L_y}{2})$ with $x \in [\frac{L_x}{2}, L_x]$

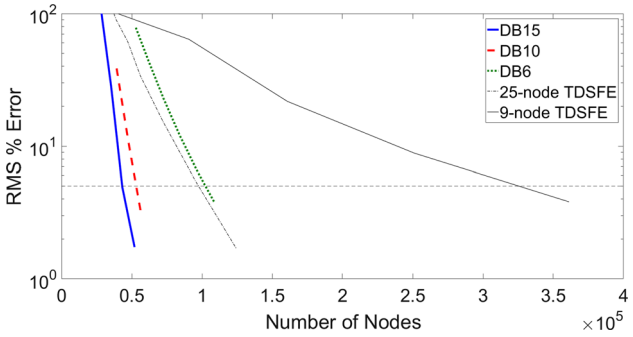

Fig. 14 Resultant RMS % error versus number of nodes for the FWD method using various DB scaling functions for the prediction of wave propagation in $[0_2/90_2]_s$ plate

case. Taking into consideration that no remeshing is required while increasing the approximation order, the FWD method provides a more satisfying performance about the modeling time and the ease of usage. On the other hand, no dramatic improvements in node size reduction were shown by comparing DB10 and DB15 Daubechies wavelets. The reason is that as the DB order increases, ill-conditioning is introduced into the calculation of connection coefficient matrices and consequently into the mass and stiffness matrices. Ill-conditioning is attributed to the high order difference in the magnitude of matrix values. Hence poor-conditioned matrices seem to limit the potential of higher order WSFs, and until matrix conditioning is improved, the best performance seems to be attained in the range of DB6-DB10 wavelets.

5 Conclusions

Taking advantage of the appealing properties of Daubechies wavelets/ scaling functions, a novel computational wavelet-based structural dynamics method, termed as finite wavelet domain method, has been developed for the prediction of high-frequency transient dynamic responses and 2D wave propagation in laminated composite plates. The formulation of the FWD method in the context of the first order shear deformation laminated plate theory is described.

Evaluation cases illustrated the ultra-high convergence rate and great reduction in discrete system sizes that emanates from the Daubechies FWD method in the simulation of antisymmetric modes at ultrasonic frequencies. The superiority of the FWD method compared to FEA in terms of accuracy, convergence rate, refinement capabilities, and computational efficiency is quantified. Three key advantages were demonstrated: (1) the ability to increase the order of approximation and decrease the problem size (p-method) without remeshing; (2) the amenability of the FWD method to explicit formulations because of the consistent diagonal mass matrices; and (3) very fast spatial convergence rates. All FWD elements have drastically outperformed the 9-node time domain spectral finite elements. The higher order FWD elements (DB15, DB10) are shown to perform better than the lower order elements (DB6).

In closing, the developed FWD method has shown great potential for applications involving demanding transient dynamic simulations, such as the analysis of wave-based SHM and NDE systems. Future work will focus on the development of FWD methods encompassing a higher order layerwise laminate theory to capture symmetric wave modes and on the inclusion of piezoelectric actuators and sensors in the formulations.

Appendix

The displacement field through the thickness according to the FSDT takes the form

$$u(x, y, z, t) = u^0(x, y, t) + \beta_x(x, y, t) \cdot z \tag{27}$$

$$v(x, y, z, t) = v^0(x, y, t) + \beta_y(x, y, t) \cdot z \tag{28}$$

$$w(x, y, z, t) = w^0(x, y, t) \tag{29}$$

where u^0, v^0, w^0 are the axial and transverse displacements at the mid-plane of the plate; β_x, β_y are the rotations of the cross-section; and z is the local thickness coordinate. The in-plane strains ε_x, ε_y, ε_{xy} and the out of plane shear strains ε_{yz}, ε_{xz} are shown below

$$\varepsilon_x(x,z,t) = \varepsilon_x^0 + k_x \cdot z \tag{30}$$

$$\varepsilon_y(y,z,t) = \varepsilon_y^0 + k_y \cdot z \tag{31}$$

$$\varepsilon_{xy}(x,y,t) = \varepsilon_{xy}^0 + k_{xy} \tag{32}$$

$$\varepsilon_{yz}(y,z,t) = \varepsilon_{yz}^0 \tag{33}$$

$$\varepsilon_{xz}(x,z,t) = \varepsilon_{xz}^0 \tag{34}$$

In the previous Eqs. (30–32), the generalized strains of the laminated plate cross section are defined as

$$\underset{\sim}{\varepsilon_L} = \begin{Bmatrix} \varepsilon_x^0 \\ \varepsilon_y^0 \\ \varepsilon_{xy}^0 \\ k_x \\ k_y \\ k_{xy} \\ \varepsilon_{yz}^0 \\ \varepsilon_{xz}^0 \end{Bmatrix} = \begin{Bmatrix} u_{,x}^0 \\ v_{,y}^0 \\ u_{,y}^0 + v_{,x}^0 \\ \beta_{x,x} \\ \beta_{y,y} \\ \beta_{x,y} + \beta_{y,x} \\ w_{,y}^0 + \beta_y \\ w_{,x}^0 + \beta_x \end{Bmatrix} \tag{35}$$

where
$\varepsilon_x^0, \varepsilon_y^0, \varepsilon_{xy}^0$ are implying membrane strains, k_x, k_y, k_{xy} are the curvatures and $\varepsilon_{yz}^0, \varepsilon_{xz}^0$ are the out of plain strains. The comma in the subscript indicates differentiation. $A's$, $B's$ and $D's$ are the extensional, bending and bending-extensional coupling stiffnesses. The principle of virtual work for a two-dimensional solid defined in terms of axial and transverse coordinates can be recast as

$$\delta V - \delta W + \delta T = 0 \tag{36}$$

where δV, δW and δT are the virtual strain energy, the virtual work induced by external applied forces and the virtual kinetic energy respectively. Each of the term in Eq. (36) is given by

$$\begin{aligned} \delta V &= \int_{\Omega_0} \left\{ \int_{-h/2}^{h/2} \left[\left(\delta\varepsilon_x + z\delta k_x\right)\sigma_{xx} + \left(\delta\varepsilon_y + z\delta k_y\right)\sigma_{yy} + \right.\right. \\ &\quad \left.\left. \left(\delta\varepsilon_{xy} + z\delta k_{xy}\right)\sigma_{xy} + \delta\varepsilon_{xz}\sigma_{xz} + \delta\varepsilon_{yz}\sigma_{yz} \right] dz \right\} dxdy \\ &= \int_{\Omega_0} \underset{\sim}{\delta\varepsilon_L^T} [\mathbf{K}_L] \underset{\sim}{\varepsilon_L} dxdy \end{aligned} \tag{37}$$

$$\begin{aligned} \delta W = \int_{\Omega_0} \delta w_0 \left[(q_b + q_t)\right] dxdy + \int_{\Gamma_\sigma} \int_{-h/2}^{h/2} \left[(\delta u_n + \right. \\ \left. z\delta\beta_n)\,\hat{\sigma}_{nn} + (\delta u_s + z\delta\beta_s)\,\hat{\sigma}_{ns} + \delta w_0 \hat{\sigma}_{nz} \right] dzds \end{aligned} \tag{38}$$

$$\begin{aligned} \delta T &= \int_{\Omega_0} \int_{-h/2}^{h/2} \rho \Big[\left(\delta u_0 + z\delta\beta_x\right)\left(\ddot{u}_0 + z\ddot{\beta}_x\right) \\ &\quad + \left(\delta v_0 + z\delta\beta_y\right)\left(\ddot{v}_0 + z\ddot{\beta}_y\right) + \delta w_0 \ddot{w}_0 \Big] dz\, dxdy \\ &= \int_{\Omega_0} \underset{\sim}{\delta u_L^T} [\boldsymbol{\rho}_L] \underset{\sim}{\ddot{u}_L} dxdy \end{aligned} \tag{39}$$

where Γ_σ denotes a portion of the boundary Γ and

$$[\mathbf{K}_L] = \begin{bmatrix} A_{11} & A_{12} & A_{16} & B_{11} & B_{12} & B_{16} & & \\ A_{12} & A_{22} & A_{26} & B_{12} & B_{22} & B_{26} & & \\ A_{16} & A_{22} & A_{66} & B_{16} & B_{26} & B_{66} & \multicolumn{2}{c}{\mathbf{0}} \\ B_{11} & B_{12} & B_{16} & D_{11} & D_{12} & D_{16} & & \\ B_{12} & B_{22} & B_{26} & D_{12} & D_{22} & D_{26} & & \\ B_{16} & B_{26} & B_{66} & D_{16} & D_{26} & D_{66} & & \\ \multicolumn{6}{c}{\mathbf{0}} & A_{44} & A_{45} \\ & & & & & & A_{45} & A_{55} \end{bmatrix} \tag{40}$$

and

$$[\boldsymbol{\rho}_L] = \begin{bmatrix} \rho_A & \rho_B & & & & \mathbf{0} \\ \rho_B & \rho_D & & & & \\ & & \rho_A & \rho_B & & \\ & & \rho_B & \rho_D & & \\ \mathbf{0} & & & & & \rho_A \end{bmatrix} \tag{41}$$

where ρ_A, ρ_B, ρ_D are the areal mass, 1st order inertia and the rotational inertia of the laminate respectively. For symmetric laminates $\rho_B = 0$.

References

1. Zienkiewicz OC, Taylor RL (2005) The finite element method for solid and structural mechanics. Butterworth-Heinemann, London
2. Strikwerda JC (2004) Finite difference schemes and partial differential equations, 2nd edn. SIAM, Philadelphia
3. Raghavan A, Cesnik CES (2007) 3-d elasticity-based modeling of anisotropic piezocomposite transducers for guided wave structural health monitoring. J Vib Acoust 129(6):739–751
4. Lingyu Y, Bottai-Santoni G, Giurgiutiu V (2010) Shear lag solution for tuning ultrasonic piezoelectric wafer active sensors with applications to lamb wave array imaging. Int J Eng Sci 48(10):848–861
5. Ahmad ZAB, Vivar-Perez JM, Gabbert U (2013) Semi-analytical finite element method for modeling of lamb wave propagation. CEAS Aeronaut J 4(1):21–33
6. Datta SK, Shah AH, Bratton RL, Chakraborty T (1988) Wave propagation in laminated composite plates. J Acoust Soc Am 83(6):2020–2026
7. Marzani A, Viola E, Bartoli I, Scalea FLD, Rizzo P (2008) A semi-analytical finite element formulation for modeling stress wave propagation in axisymmetric damped waveguides. J Sound Vib 318(3):488–505
8. Patera AT (1984) A spectral element method for fluid dynamics: laminar flow in a channel expansion. J Comput Phys 54(3):468–488
9. Kudela P, Krawczuk M, Ostachowicz W (2007) Wave propagation modelling in 1d structures using spectral finite elements. J Sound Vib 300(1):88–100

10. Monasse P, Perrier V (1998) Orthonormal wavelet bases adapted for partial differential equations with boundary conditions. SIAM J Math Anal 29(4):1040–1065
11. Qian S, Weiss J (1993) Wavelets and the numerical solution of boundary value problems. Appl Math Lett 6(1):47–52
12. Li B, Chen X (2014) Wavelet-based numerical analysis: a review and classification. Finite Elem Anal Des 81:14–31
13. Patton R, Marks P (1995) The rod finite element, a new type of finite element. In: 36th structures, structural dynamics and materials conference: structures, structural dynamics, and materials and co-located conferences. American Institute of Aeronautics and Astronautics
14. Patton R, Marks P (1995) Application of the rod wavelet finite element to dynamic systems. In: 36th structures, structural dynamics and materials conference: structures, structural dynamics, and materials and co-located conferences. American Institute of Aeronautics and Astronautics
15. Ma J, Xue J, Yang S, He Z (2003) A study of the construction and application of a daubechies wavelet-based beam element. Finite Elem Anal Des 39(10):965–975
16. Chen X, Yang S, Ma J, He Z (2004) The construction of wavelet finite element and its application. Finite Elem Anal Des 40(5):541–554
17. Zhou Y-H, Zhou J (2008) A modified wavelet approximation of deflections for solving pdes of beams and square thin plates. Finite Elem Anal Des 44(12):773–783
18. Díaz LA, Martín MT, Vampa V (2009) Daubechies wavelet beam and plate finite elements. Finite Elem Anal Des 45(3):200–209
19. Mitra M, Gopalakrishnan S (2005) Spectrally formulated wavelet finite element for wave propagation and impact force identification in connected 1-D waveguides. Int J Solids Struct 42(16):4695–4721
20. Samaratunga D, Jha R, Gopalakrishnan S (2014) Wavelet spectral finite element for wave propagation in shear deformable laminated composite plates. Compos Struct 108:341–353
21. Burgos RB, Santos MAC, e Silva RR (2013) Deslauriers–Dubuc interpolating wavelet beam finite element. Finite Elem Anal Des 75:71–77
22. Xiang JW, Chen XF, He ZJ, Dong HB (2007) The construction of 1d wavelet finite elements for structural analysis. Comput Mech 40(2):325–339
23. Zuo H, Yang Z, Chen X, Xie Y, Miao H (2015) Analysis of laminated composite plates using wavelet finite element method and higher-order plate theory. Compos Struct 131:248–258
24. Zhang X, Chen X, Wang X, He Z (2010) Multivariable finite elements based on b-spline wavelet on the interval for thin plate static and vibration analysis. Finite Elem Anal Des 46(5):416–427
25. Theodosiou T, Nastos C, Rekatsinas C, Saravanos D (2014) Finite wavelet domain method for efficient modeling of lamb wave based structural health monitoring. In: EWSHM-7th European workshop on structural health monitoring, Nantes, France
26. Nastos CV, Theodosiou TC, Rekatsinas CS, Saravanos DA (2015) A finite wavelet domain method for the rapid analysis of transient dynamic response in rods and beams. CMES Comput Model Eng Sci 107(5):379–409
27. Reddy JN (2004) Mechanics of laminated composite plates and shells: theory and analysis. CRC Press, Boca Raton
28. Daubechies I (1992) Ten Lectures on Wavelets, CBMS-NSF Regional Conference Series in Applied Mathematics, vol 61. SIAM, Philadelphia
29. Lin W, Kovvali N, Carin L (2005) Direct algorithm for computation of derivatives of the daubechies basis functions. Appl Math Comput 170(2):1006–1013
30. CHEN M-Q, Hwang C, SHIH Y-P (1996) The computation of wavelet-galerkin approximation on a bounded interval. Int J Numer Meth Eng 39(17):2921–2944
31. Ko J, Kurdila AJ, Pilant MS (1995) A class of finite element methods based on orthonormal, compactly supported wavelets. Comput Mech 16(4):235–244
32. Beylkin G (1992) On the representation of operators in bases of compactly supported wavelets. SIAM J Numer Anal 29(6):1716–1740
33. Zhang T, Tian Y-C, Tadé MO, Utomo J (2007) Comments on "the computation of wavelet-galerkin approximation on a bounded interval". Int J Numer Meth Eng 72(2):244–251
34. Rekatsinas CS, Nastos CV, Theodosiou TC, Saravanos DA (2015) A time-domain high-order spectral finite element for the simulation of symmetric and anti-symmetric guided waves in laminated composite strips. Wave Motion 53:1–19
35. Barouni AK (2016) A layerwise semi-analytical method for modeling guided wave propagation in laminated and sandwich composite strips with induced surface excitation. Aerosp Sci Technol 51:118–141